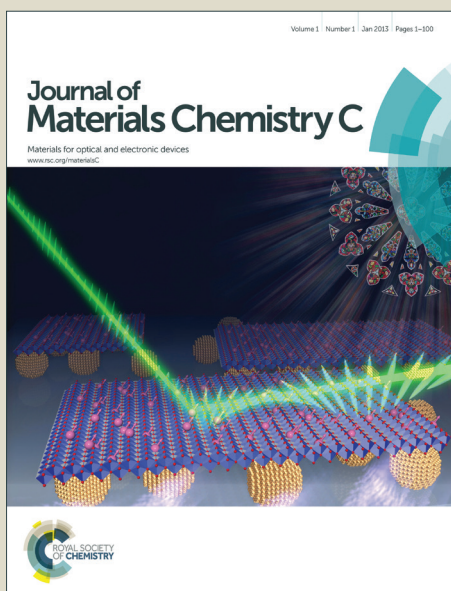


Journal of Materials Chemistry C

Accepted Manuscript



This is an *Accepted Manuscript*, which has been through the Royal Society of Chemistry peer review process and has been accepted for publication.

Accepted Manuscripts are published online shortly after acceptance, before technical editing, formatting and proof reading. Using this free service, authors can make their results available to the community, in citable form, before we publish the edited article. We will replace this *Accepted Manuscript* with the edited and formatted *Advance Article* as soon as it is available.

You can find more information about *Accepted Manuscripts* in the [Information for Authors](#).

Please note that technical editing may introduce minor changes to the text and/or graphics, which may alter content. The journal's standard [Terms & Conditions](#) and the [Ethical guidelines](#) still apply. In no event shall the Royal Society of Chemistry be held responsible for any errors or omissions in this *Accepted Manuscript* or any consequences arising from the use of any information it contains.

Chemical trends of Mn^{4+} emission in solides

Mao-Hua Du

Materials Science & Technology Division, Oak Ridge, TN 37831, USA

Mn^{4+} is known to activate red emission in many materials. However, the existing Mn^{4+} activated red phosphors have relatively long emission wavelengths and are therefore inefficient for general lighting purposes. Density functional calculations are performed on a large number of Mn^{4+} doped materials with diverse crystal structures to understand how material properties of different hosts affect the emission energy of the Mn^{4+} dopant. The results show that weak Mn^{4+} -ligand hybridization generally leads to higher Mn^{4+} emission energies. Host materials allowing long Mn-ligand distance and/or significant distortion of bond angles around the Mn octahedral site are shown to have higher emission energies. Several new oxide host materials are found for Mn^{4+} . Their emission energies are found to be higher than those currently known for Mn^{4+} doped oxides and should be closer to that of $\text{Y}_2\text{O}_3:\text{Eu}^{3+}$, which is the current commercial red phosphor for fluorescent lighting.

PACS: 61.72.S-, 71.55.Ht

I. Introduction

Efficient luminescence in inorganic semiconductors and insulators usually relies on the localization of excited electrons and holes at activators, which are impurities acting as luminescence centers. Commonly used activators are typically multivalent ions, which can insert multiple electronic states inside the band gap of wide-gap materials.^{1 2} These gap states trap electrons and holes, leading to radiative recombination. Good examples of the multivalent ions that can act as luminescent centers are rare-earth (e.g., Ce^{3+} , Eu^{2+}),^{3 4 5 6 7 8} transition metal (e.g., Cr^{3+} , Mn^{4+}),^{9 10} and ns^2 ions.^{11 12 13}

Rare-earth activators are most widely used in phosphors for energy efficient lighting (e.g., fluorescent lamps and white LEDs).¹⁴ However, alternative activators and their suitable hosts are also being pursued for higher efficiency and lower cost.¹⁵ Supply constraint of the rare-earth elements further increases the urgency of developing rare-earth-free phosphors for lighting and other optoelectronic applications. The development of new efficient and inexpensive red phosphors is of particular interest because the current commercial red phosphor, i.e., $\text{Y}_2\text{O}_3:\text{Eu}^{3+}$, is the most expensive component of the triphosphor blend in fluorescent lamps.¹⁴

Mn^{4+} doped materials have been extensively studied for lighting,¹⁵ holography,¹⁶ laser,¹⁷ and dosimetry¹⁸. There is a long list of Mn^{4+} activated red-emitting phosphors, including SrTiO_3 ,¹⁹ Al_2O_3 ,²⁰ YAlO_3 ,¹⁷ $\text{Gd}_3\text{Ga}_5\text{O}_{12}$,²¹ CaZrO_3 ,²² $\text{Y}_2\text{Sn}_2\text{O}_7$,¹⁰ MgO ,²³ K_2SiF_6 ,^{24 25} Na_2SiF_6 ,²⁶ Na_2SnF_6 ,²⁷ and Cs_2SnF_6 .²⁷ Brik and Srivastava compiled a list of Mn^{4+} activated phosphors and their emission wavelengths.⁹ The Mn^{4+} emission wavelengths of these phosphors are all longer than that of $\text{Y}_2\text{O}_3:\text{Eu}^{3+}$ (611 nm).⁹ Currently, the closest Mn^{4+} emission wavelength to that of $\text{Y}_2\text{O}_3:\text{Eu}^{3+}$ is 617 nm for

Na_2SiF_6 .²⁶ The Mn^{4+} activated fluoride phosphors have recently attracted considerable interest due to their potential use as red phosphors in LED devices.^{24,25,26,27} However, the fluoride phosphors are not suitable for use in fluorescent lamps due to their reactivity with the mercury vapor present in fluorescent lamps. The Mn^{4+} emission wavelengths of more chemically stable oxide phosphors are longer than those of fluorides.⁹ The shortest reported Mn^{4+} emission wavelength in oxides is 648 nm for $\text{Y}_2\text{Sn}_2\text{O}_7$.¹⁰ It is important to note that human eye sensitivity to red light decreases rapidly when the emission wavelength goes above 611 nm (by more than 60% from 611 to 648 nm). Hence, the currently known Mn^{4+} activated oxide phosphors are inefficient for general lighting. Designing new Mn^{4+} activated oxide phosphors with shorter emission wavelengths for fluorescent lighting requires fundamental understanding of the material properties that govern the Mn^{4+} emission.

Mn^{4+} is a $3d^3$ ion. In an octahedral environment, the Mn-3d states are split into three- and two-fold degenerate t_{2g} and e_g states, respectively. The three Mn-3d electrons of Mn^{4+} exactly fill the majority-spin t_{2g} states. The crystal field splitting creates a large gap between the t_{2g} and e_g states, stabilizing the 4+ oxidation state [Fig. 1(a)]. Therefore, Mn^{4+} is usually found on octahedral sites of solids. The emission spectrum of Mn^{4+} typically shows a sharp line corresponding to the spin- and parity-forbidden ${}^2E_g \rightarrow {}^4A_{2g}$ transition. This emission is nearly independent of the crystal field splitting according to the Tanabe-Sugano diagram.^{28,29} However, variation of the Mn^{4+} emission energy in different hosts is still significant.⁹ It is observed that the ${}^2E_g \rightarrow {}^4A_{2g}$ emission energy of Mn^{4+} tends to increase with Racah parameter B , which decreases with stronger Mn-ligand hybridization.^{9,22} This is an important trend and can explain the higher ${}^2E_g \rightarrow {}^4A_{2g}$

emission energies of Mn^{4+} in fluorides than in oxides by recognizing the weaker Mn-ligand hybridization in fluorides.

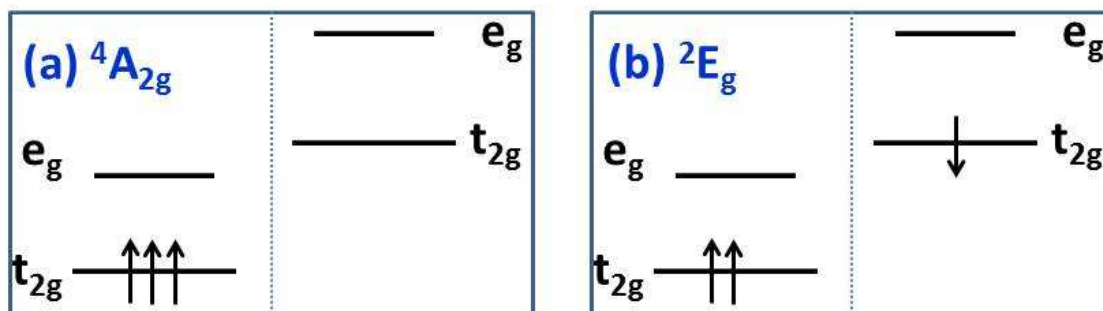


FIGURE 1. Single-particle schematic diagrams of (a) the ${}^4A_{2g}$ ground state and (b) the 2E_g excited state of Mn^{4+} in an octahedral environment. Note that the Jahn-Teller splitting of the partially occupied levels in 2E_g state is not shown.

The exchange charge model of crystal field³⁰ has been used to study the absorption and emission of Mn^{4+} in different host materials.^{9,10,22} The crystal environment is incorporated by considering both the electrostatic potential by a large number of lattice ions (point charges) and the wavefunction overlaps between Mn^{4+} 3d states and ligand s and p states. This method employs multi-electronic wavefunctions and can be used to calculate the transition energy between multi-electron states. By fitting a few parameters (which could be reduced to one with appropriate approximations) to experimentally measured absorption bands, one can obtain absorption and emission energies of Mn^{4+} in reasonable agreement with experimental results.^{9,10,22} The main drawbacks of this method are that (1) it is not a predictive theory and requires parameter fitting and that (2) it does not consider structural relaxation around Mn^{4+} (which is shown to be important in this study) and the treatment of Mn-ligand interaction is not sufficiently accurate.

In this work, density functional theory (DFT)³¹ with standard Perdew-Burke-Ernzerhof (PBE)³² is used to study the Mn⁴⁺ emission. The goal is to understand the trend of Mn⁴⁺ emission energies in various oxide and fluoride hosts and identify simple criteria for searching new host materials for Mn⁴⁺ with suitable emission energies for fluorescent lighting. The Mn⁴⁺ emission energy is calculated by taking the energy difference between the low-spin and the high-spin states of Mn⁴⁺. The low and high spin states have the magnetic moments of $1\mu_B$ and $3\mu_B$, respectively, as schematically shown in Fig. 1. Fig. 1(a) and (b) are the single-particle representations of the ${}^4A_{2g}$ and 2E_g states used in the calculations. For convenience, the multi-electron notations, i.e., ${}^4A_{2g}$ and 2E_g , are used to label the single-particle ground and emitting states throughout this paper.

DFT is a ground-state single-particle theory, which in principle is incapable of calculating the transition energy between multi-electron states. Including nonlocal correlation effects by using hybrid functionals^{33, 34} does not solve the intrinsic problem of DFT as a ground state theory in describing excited state properties. Nevertheless, the DFT-PBE method has several advantages, i.e., (1) it provides full structural relaxation and good treatment of Mn-ligand hybridization and that (2) it is an efficient method enabling fast screening of a large number of materials. Previous work has shown that the variation of the Mn⁴⁺ emission energy in different hosts is caused by the different Mn-ligand hybridization strengths,⁹ which can be distinguished by DFT calculations as shown in this work. Therefore, DFT calculations should produce a correct trend of Mn⁴⁺ emission energies despite that the absolute value of the calculated emission energy is not expected to be correct. Establishing a correct trend is very useful because it enables the identification of new Mn⁴⁺ activated red phosphors with emission energies higher and

closer to that of $\text{Y}_2\text{O}_3:\text{Eu}^{3+}$ than those currently known. Carefully examining DFT-calculated Mn^{4+} emission energies and DFT-relaxed structures can reveal important structural factors that lead to the weakening of the Mn-ligand hybridization and consequently higher emission energy.

In this paper, the Mn^{4+} emission energy is calculated for a large number of oxide and fluoride hosts using DFT calculations. Many different structural forms, including perovskite, rock salt, pyrochlore, bixbyite, etc., which all have octahedral or distorted octahedral sites for Mn doping, have been investigated. Oxide hosts are of particular interest due to their stability in the mercury environment in fluorescent lamps.

The calculated Mn^{4+} emission energies based on DFT-PBE method are found to be significantly lower than those measured experimentally, as expected. However, PBE calculations of a large number of oxide and fluoride hosts produce a trend for Mn^{4+} emission energies consistent with the experimental results. Extensive data from this study confirms previous observation⁹ that decreasing hybridization between the Mn^{4+} ion and its ligands can increase the emission energy. This trend can be understood in a single-particle picture considering different Mn-ligand hybridization in the ground and the emitting states. Increasing Mn-ligand distance and distorting bond angles around the Mn octahedral site both lead to weakened Mn-ligand hybridization and higher Mn^{4+} emission energies. The bond angle distortion plays an important role as reflected by the generally higher emission energies in pyrochlores (with large bond angle distortion in MnO_6 octahedrons) than in perovskites (with small or no bond angle distortion in MnO_6 octahedrons). Several new Mn^{4+} activated red-emitting phosphors are proposed based on

the calculations. Hybrid functional calculations of Mn^{4+} emission energies are also discussed.

II. Computational details

Density functional calculations with PBE functionals³² were performed using the VASP codes.^{35, 36} The valence wavefunctions were expanded in a plane-wave basis with a cut-off energy of 400 eV. All the atoms were relaxed to minimize the Feynman-Hellmann forces to below 0.02 eV/Å. The Mn^{4+} emission energy is calculated by

$$\Delta E_{em} = E(1\mu_B) - E(3\mu_B), \quad (1)$$

where $E(1\mu_B)$ and $E(3\mu_B)$ are the total energies of structurally relaxed low-spin ($1\mu_B$) and high-spin ($3\mu_B$) states of Mn^{4+} as schematically shown in Fig. 1. Heyd-Scuseria-Ernzerhof (HSE06) hybrid functionals^{33, 34} are also used for calculating the Mn^{4+} emission energies and band gaps of selected materials.

III. Results

A. Mn-ligand hybridization

$\text{K}_2\text{SiF}_6:\text{Mn}^{4+}$ is used here as an example for Mn^{4+} in an octahedral environment. Figure 2 shows the density of states (DOS) for Mn^{4+} doped K_2SiF_6 calculated using DFT-PBE method. K_2SiF_6 has a cubic structure (space group Fm3m). The ${}^4\text{A}_{2g}$ ground state has the octahedral symmetry while the ${}^2\text{E}_g$ excited state undergoes small Jahn-Teller distortion to assume the tetragonal symmetry, which leads to the splitting of the t_{2g} and the e_g levels as shown in Fig. 2(b).

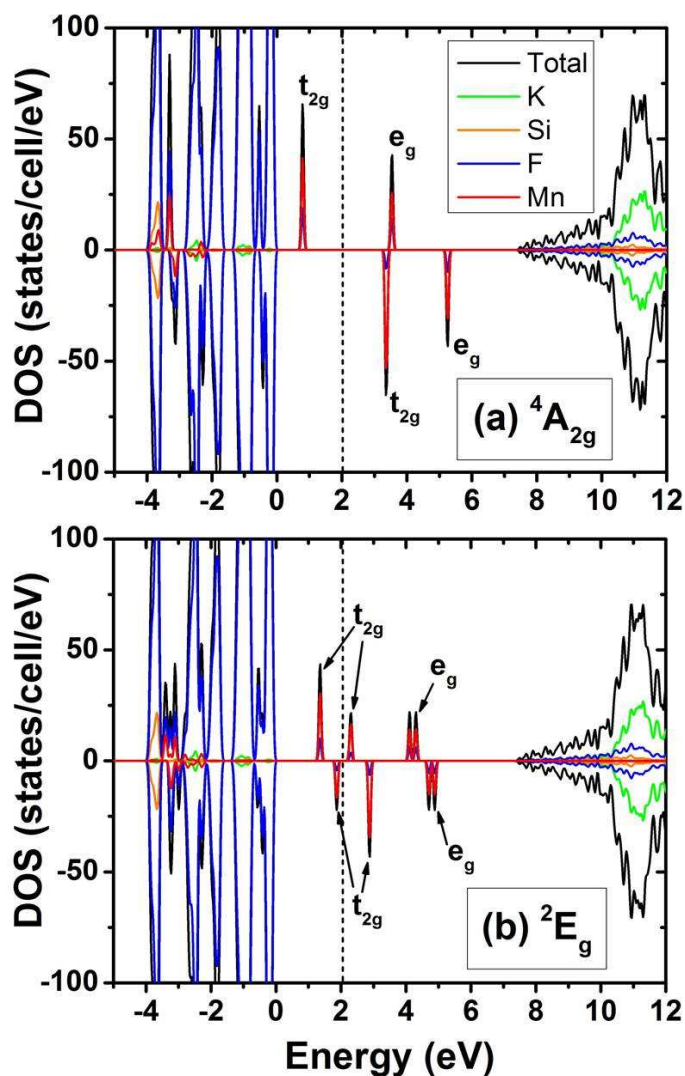


FIGURE 2. Density of states (DOS) for Mn^{4+} doped K_2SiF_6 calculated using DFT-PBE method. The DOS is projected onto different atomic types. The ground state ${}^4\text{A}_{2g}$ is shown in (a) and the excited state ${}^2\text{E}_g$ is shown in (b). The dashed line separates the occupied states (to the left) and the unoccupied states (to the right).

Both t_{2g} and e_g states of Mn hybridize with the ligand-p states as can be seen in Fig. 2 for K_2SiF_6 , where both the Mn 3d and the F 2p states contribute to the t_{2g} and e_g states in the band gap. The Mn^{4+} emission [transition from Fig. 1(b) to Fig. 1(a)] involves only a spin flip from the minority-spin t_{2g} to the majority-spin t_{2g} state. Therefore, the emission energy is nearly independent of both the crystal field splitting and the

hybridization that involves e_g states. The Mn-ligand hybridization strengths in ${}^4A_{2g}$ and 2E_g states are about the same since the average t_{2g} and e_g orbital energies (averaging over both majority and minority spins) do not change from ${}^4A_{2g}$ to 2E_g as may be seen in Fig. 2. However, the hybridization between the filled ligand-p states in the valence band and the empty t_{2g} states should increase from ${}^4A_{2g}$ to 2E_g , because the three empty t_{2g} states of 2E_g are lower and thus closer in energy to the ligand-p states than the three empty t_{2g} states of ${}^4A_{2g}$. (The p-d hybridization tends to increase when the p and d states are closer in energy to each other.) Since only the hybridization between the filled ligand-p states and the empty Mn-3d states lowers the total energy, the Mn-ligand hybridization lowers the total energy of 2E_g more than that of ${}^4A_{2g}$, which reduces the ${}^2E_g \rightarrow {}^4A_{2g}$ emission energy. This should lead to the general trend of increasing emission energy with decreasing hybridization between Mn^{4+} and its ligands. This point is further demonstrated by numerical calculations shown in Sec. III-B.

B. Mn^{4+} emission energy

The Mn^{4+} emission energies for several oxide and fluoride hosts with known experimental data are calculated using the DFT-PBE method (Fig. 3). It can be seen that PBE-calculated emission energies are significantly lower than the experimental ones. However, the emission energy trend is reproduced well by the PBE calculations except for the transition from oxides to fluorides. The lack of a jump in the calculated emission energy when transitioning from oxides to fluorides in Fig. 3 is likely due to that the self-interaction error (larger in fluorides than in oxides) in the PBE calculation that makes fluorides appear more covalent, which increases the hybridization and lowers the

emission energy. The Mn^{4+} emission energy trend is described very well by the DFT-PBE method if the ligands in all host materials are the same. The DFT-PBE method can better distinguish the different Mn-ligand hybridization strengths if the variation is caused by different bonding configurations rather than different electronegativities of the ligands. The variation of the Mn^{4+} emission energy is smaller in fluorides than in oxides (see Fig. 3 and Ref. 9). This is likely because the Mn-F hybridization is generally very weak and its variation in different fluorides is not significant.

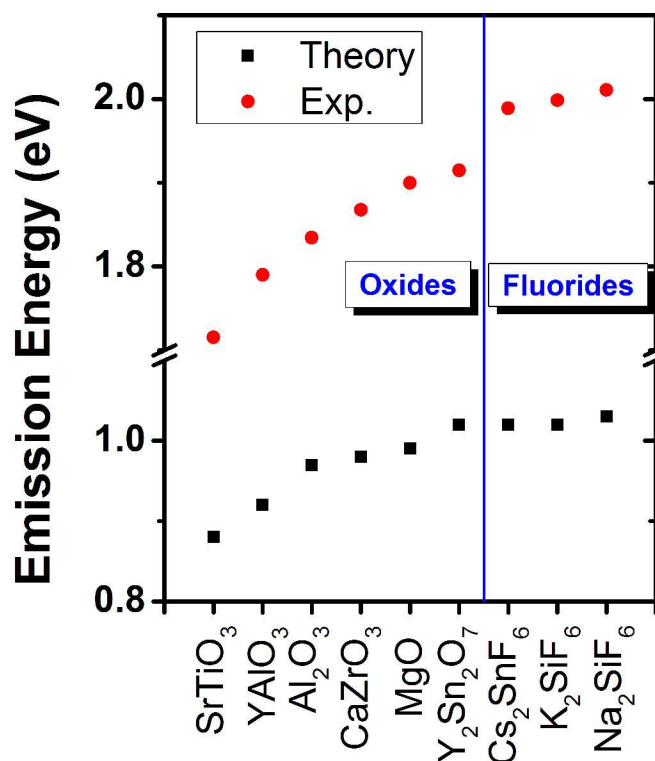


FIGURE 3. (Color online) Experimental and theoretical values of Mn^{4+} emission energies for a number of oxides and fluorides. The theoretical values are obtained by DFT-PBE calculations.

Table I. Calculated (by DFT-PBE method) Mn^{4+} emission energies for various oxides and fluorides. The experimentally observed Mn^{4+} emission energies (zero phone lines) are shown wherever available. The Mn substitutional sites and their charge states are also shown.

		DFT-PBE (eV)	Exp. (eV)
SrTiO_3	Mn_{Ti}^0	0.88	1.716 (Ref. 19)
SrHfO_3	Mn_{Hf}^0	0.97	
YAlO_3	Mn_{Al}^+	0.92	1.791 (Ref. 17)
BaSnO_3	Mn_{Sn}^0	0.94	
CaZrO_3	Mn_{Zr}^0	0.98	1.868 (Ref. 22)
MgTa_2O_5	Mn_{Ta}^-	0.94	
MgO	$\text{Mn}_{\text{Mg}}^{2+}$	0.99	1.903 (Ref. 23)
CaO	$\text{Mn}_{\text{Ca}}^{2+}$	1.02	
SrO	$\text{Mn}_{\text{Sr}}^{2+}$	1.03	
BaO	$\text{Mn}_{\text{Ba}}^{2+}$	1.04	
Al_2O_3	Mn_{Al}^+	0.97	1.835 (Ref. 20)
Ga_2O_3 ³⁷	Mn_{Ga}^+	0.97	
In_2O_3 ³⁸	Mn_{In}^+	1.01	
Y_2O_3 ³⁸	Mn_{Y}^+	1.05	
$\text{Y}_2\text{Ti}_2\text{O}_7$	Mn_{Ti}^0	1.01	
$\text{Y}_2\text{Sn}_2\text{O}_7$	Mn_{Sn}^0	1.02	1.915 (Ref. 10)
$\text{La}_2\text{Sn}_2\text{O}_7$	Mn_{Sn}^0	1.03	
$\text{La}_2\text{Zr}_2\text{O}_7$	Mn_{Zr}^0	1.03	
K_2SiF_6	Mn_{Si}^0	1.02	1.999 (Ref. 25)
Na_2SiF_6 ³⁹	Mn_{Si}^0	1.03	2.011(Ref. 26)
Cs_2SnF_6	Mn_{Sn}^0	1.02	1.989 (Ref. 27)
Cs_2ZrF_6	Mn_{Zr}^0	1.03	
ZrP_2O_7	Mn_{Zr}^0	0.84	
$\text{BaZr}(\text{PO}_4)_2$	Mn_{Zr}^0	0.96	

Table I shows the PBE-calculated ${}^2\text{E} \rightarrow {}^4\text{A}_2$ emission energy of Mn^{4+} for a large number of oxides and fluorides. Despite their diverse crystal structures, these materials

all contain octahedral or distorted octahedral lattice sites for stabilizing Mn^{4+} . Many of these compounds have not been studied experimentally as hosts for Mn^{4+} . The emission energies of Mn^{4+} in new host materials are calculated and compared with the existing ones, for which the experimental data are available. Since PBE calculations can produce a good trend of Mn^{4+} emission energies in different oxide hosts (see Fig. 3), this approach can identify new oxide host materials with emission energies higher than those currently known.

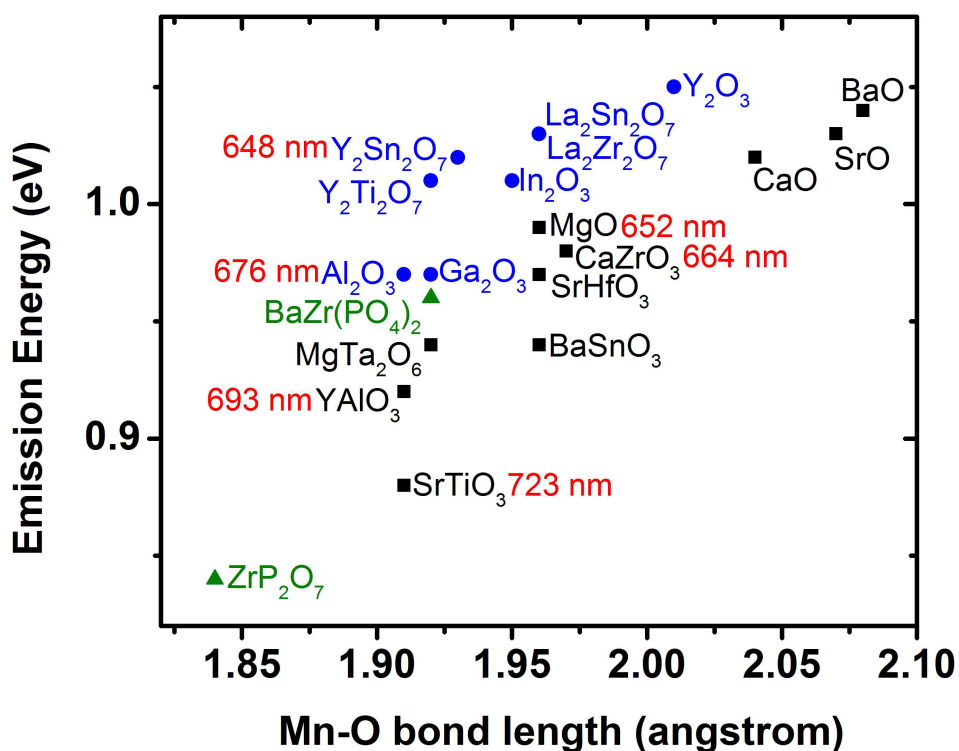


FIGURE 4. (Color online) PBE-calculated Mn^{4+} emission energies for various oxides as functions of Mn-O bond length. The Mn-O bond length is the average over the six Mn-O bond lengths in the MnO_6 octahedron. The experimental values are shown (in red) wherever available. Note that the calculated Mn-O bond lengths and emission energies for $\text{La}_2\text{Zr}_2\text{O}_7$ and $\text{La}_2\text{Sn}_2\text{O}_7$ are the same. There are three groups of materials in the figure: the ones with small O-Mn-O bond angle distortion (black squares), the ones with large O-Mn-O bond angle distortion (blue circles), and phosphates (green triangles). See text for details of these different groups of materials.

Fig. 4 shows the calculated Mn^{4+} emission energies for the oxide hosts in Table I as a function of Mn-O bond length. Several important observations can be made from the results in Fig. 4:

(1) Several Mn^{4+} -activated oxide phosphors (e.g., Y_2O_3 , $\text{La}_2\text{Zr}_2\text{O}_7$, and $\text{La}_2\text{Sn}_2\text{O}_7$) are shown to exhibit higher emission energies than $\text{Y}_2\text{Sn}_2\text{O}_7:\text{Mn}^{4+}$, which currently has the highest experimentally measured Mn^{4+} emission energy in oxides. These emission energies, although not accurately predicted by the PBE calculations, should be closer to that of $\text{Y}_2\text{O}_3:\text{Eu}^{3+}$ (the commercial red phosphor for fluorescent lighting) than those of existing oxide phosphors.

(2) Longer Mn-O bond length generally leads to higher emission energy, or shorter wavelength, due to weaker hybridization between the Mn 3d (t_{2g}) states and the O-2p states. This trend is most evident among hosts of the same structural form. For example, the Mn^{4+} emission energy increases from MgO, CaO, SrO, to BaO, from In_2O_3 to Y_2O_3 , and from $\text{Y}_2\text{Ti}_2\text{O}_7$ to $\text{Y}_2\text{Sn}_2\text{O}_7$, as can be seen in Fig. 4. Among the materials of same structural form, those having large cation sites for Mn^{4+} substitution exhibit longer Mn-O bond lengths and higher emission energies. However, this rule is quickly violated when comparing materials of different structural forms. For examples, the calculated Mn^{4+} emission energy of $\text{Y}_2\text{Ti}_2\text{O}_7:\text{Mn}^{4+}$ is higher than those of $\text{CaZrO}_3:\text{Mn}^{4+}$ and $\text{ZrP}_2\text{O}_7:\text{Mn}^{4+}$ although Ti^{4+} is smaller than Zr^{4+} . These exceptions are discussed below.

(3) The distortion of the MnO_6 octahedron affects the Mn-O hybridization. The results in Fig. 4 combined with structural analyses suggest that the Mn^{4+} emission energy increases if the O-Mn-O angle in MnO_6 octahedrons deviates from 90° . To better

illustrate this trend, the materials shown in Fig. 4 are separated into three groups (shown in black squares, blue circles, and green triangles). The group represented by black squares and blue circles are those with small and large O-Mn-O bond angle distortions in MnO_6 octahedrons, respectively. The former have either perovskite or rock-salt structures with small ($<2^\circ$) or no O-Mn-O bond angle distortion, while the latter are pyrochlores or oxides of trivalent metals (i.e., Al, Ga, In, Y) with bond angle distortion larger than 4° . The O-Mn-O bond angle is 90° in cubic perovskites (e.g., SrTiO_3 , BaSnO_3) and in alkali-earth metal oxides of rock-salt structures, and is only slightly distorted from 90° in orthorhombic perovskite (e.g., $<2^\circ$ in CaZrO_3). In contrast, the deviation of the O-Mn-O bond angles from 90° is significant in pyrochlores, reaching more than 8° in the case of $\text{Y}_2\text{Sn}_2\text{O}_7$ for instance. Analyses of the wavefunctions of Mn-3d states in $\text{Y}_2\text{Sn}_2\text{O}_7:\text{Mn}^{4+}$ shows that the O-Mn-O bond angle distortion forces the d_{xy} , d_{yz} , and d_{xz} orbitals of t_{2g} to move out of the MnO_4 plane. This should reduce the hybridization between the Mn-3d (t_{2g}) states and the O-2p orbitals. The weakened Mn-O hybridization in pyrochlores compared to that in perovskites explains the higher Mn^{4+} emission energies of $\text{Y}_2\text{Ti}_2\text{O}_7$, $\text{Y}_2\text{Sn}_2\text{O}_7$ and $\text{La}_2\text{Zr}_2\text{O}_7$ (pyrochlores) than those of SrTiO_3 , BaSnO_3 and CaZrO_3 (perovskites). The O-Mn-O bond angles in Al_2O_3 , Ga_2O_3 , In_2O_3 , and Y_2O_3 also have significant distortions from 90° (e.g., $\sim 9^\circ$ in $\text{Al}_2\text{O}_3:\text{Mn}^{4+}$), which lead to higher Mn^{4+} emission energies. For example, due to the larger O-Mn-O bond angle distortion in Al_2O_3 ($\sim 9^\circ$) than in perovskite YAlO_3 ($<1^\circ$), the emission energy of $\text{Al}_2\text{O}_3:\text{Mn}^{4+}$ is significantly higher than that of $\text{YAlO}_3:\text{Mn}^{4+}$ although in both materials Mn^{4+} occupies the Al^{3+} site and the Mn-O bond lengths are nearly the same. It can be seen in Fig. 4 that, when comparing Mn^{4+} emission energies among materials with similar Mn-O bond lengths, the

materials with larger O-Mn-O bond angle distortion (blue circles) generally exhibit higher emission energies than those with small bond angle distortion (black squares).

(4) Zirconium phosphates are the third group of host materials for Mn^{4+} in Fig. 4 (green triangles). The strong P-O covalent bonding should lower the O-2p-derived valence band⁴⁰ and thus increases the energy separation between the Mn 3d (t_{2g}) states and the ligand-p states. Therefore, it was initially thought that the Mn-O hybridization strength should be weaker and hence the Mn^{4+} emission energy should be higher in phosphates than in oxides. However, the calculated Mn^{4+} emission energies in zirconium phosphates [i.e., $\text{BaZr}(\text{PO}_4)_2$ and ZrP_2O_7] are actually lower than those of zirconates. The reason is found to be that the metal-oxygen bond length is quite flexible in these phosphates although the $(\text{PO}_4)^{3-}$ tetrahedrons are very rigid. In phosphates such as $\text{BaZr}(\text{PO}_4)_2$, the $(\text{PO}_4)^{3-}$ tetrahedrons are connected through metal ions. In pyrophosphates such as ZrP_2O_7 , every two PO_4 tetrahedrons are connected by sharing one O ion forming $(\text{P}_2\text{O}_7)^{4-}$. The $(\text{P}_2\text{O}_7)^{4-}$ double-tetrahedra are further linked through metal ions. When a smaller Mn^{4+} ion replaces a larger Zr^{4+} ion in zirconium phosphates, the nearby metal-O bonds (such as Zr-O bonds) are simply elongated to allow substantial structural relaxation around Mn and the formation of short Mn-O bonds. The Mn-O bond lengths in zirconium phosphates are shorter than those in zirconium based perovskites and pyrochlores as shown in Fig. 4. The short Mn-O bonds in phosphates lead to strong hybridization and relatively low emission energies. The calculations on phosphates highlight the importance of structural relaxation to the Mn^{4+} emission energy. The O-Mn-O bond angle distortions are $<2^\circ$ and $<4^\circ$ in ZrP_2O_7 and $\text{BaZr}(\text{PO}_4)_2$, respectively. ZrP_2O_7 can be grouped into the hosts with small O-Mn-O bond angle distortion (black squares in

Fig. 4) while $\text{BaZr}(\text{PO}_4)_2$ has intermediate bond angle distortion between those shown in black squares and blue circles in Fig. 4.

IV. Discussion

The present study is focused on establishing chemical trends for Mn^{4+} emission in the octahedral environment. Detailed energetics, solubility, and oxidation state of Mn^{4+} and optical absorption of Mn^{4+} are beyond the scope of this study. However, comments can be made on several important issues that must be considered for designing new Mn^{4+} activated red phosphors.

(1) When Mn^{4+} is introduced as donors or acceptors (e.g., Mn^{4+} is a donor in $\text{Y}_2\text{O}_3:\text{Mn}^{4+}$), doping with compensating dopants is needed to stabilize the 4+ oxidation state of Mn and to ensure a large Mn^{4+} concentration.

(2) The across-band-gap excitation usually leads to significant energy loss through non-radiative recombination. High-quantum-yield phosphors should be designed such that the excitation occurs directly at the activator or by charge transfer mechanism (an electron is excited from the ligand ion to the activator). The UV emission from mercury vapor is used in fluorescent lamps as excitation source for phosphors. The main emission from the mercury vapor is 254 nm (4.88 eV). Thus, the phosphors for fluorescent lighting should have an optical band gap larger than 4.88 eV. This requirement favors the large-gap oxides such as Y_2O_3 and $\text{La}_2\text{Zr}_2\text{O}_7$ with HSE06 calculated band gaps of 5.71 and 5.68 eV, respectively. The experimental band gap for Y_2O_3 is about 6 eV,⁴¹ in good agreement with the calculated value (5.71 eV). The

HSE06-calculated band gaps for $\text{Y}_2\text{Sn}_2\text{O}_7$ and $\text{La}_2\text{Sn}_2\text{O}_7$ are smaller. They are 4.67 and 4.49 eV, respectively.

(3) The targeted emission energy for red phosphors is around 611 nm (2.03 eV). A large Stokes shift of more than 2.85 eV (4.88 – 2.03 eV) on Mn^{4+} seems difficult to obtain. In other words, the absorption of Mn^{4+} at 488 eV is probably weak in most hosts. Additional dopants may be introduced into the phosphor as sensitizers, which absorb the high energy photons from mercury vapor and then transfer the energy to Mn^{4+} . Alternatively, charge transfer type of excitation can be invoked for efficient absorption of mercury emission. In this case, the onset of excitation from the valence band to the excited state of Mn^{4+} should be less than 4.88 eV.

(4) Chemical stability in the operating and manufacturing environments of phosphors should be considered. The phosphors used in fluorescent lamps should not react with mercury or water. For example, silicates react with mercury and alkali-earth oxides react to water and thus both are not suitable for use in fluorescent lamps.

Table II. Calculated (using PBE and HSE06 functionals) and experimentally measured Mn^{4+} emission energies.

	PBE (eV)	HSE06 (eV)	Exp. (eV)
SrTiO_3	0.88	1.23	1.716
Al_2O_3	0.97	1.29	1.835
SrHfO_3	0.97	1.30	
K_2SiF_6	1.02	1.29	1.999

Finally, I comment on the effect of using hybrid functionals on the Mn^{4+} emission energy. The PBE calculation places the minority-spin t_{2g} level below the majority-spin e_g level for Mn^{4+} , consistent with the LDA calculations for Cr^{3+} (isoelectronic to Mn^{4+}) in Al_2O_3 .⁴² More advanced HSE06 calculation, which has been shown to improve the description of transition metal perovskites,^{43 44} places the minority-spin t_{2g} level above the majority-spin e_g level and increases the energy gap between the t_{2g} and the e_g levels for Mn^{4+} . Therefore, the HSE06 calculation yields higher Mn^{4+} emission energy than the PBE calculation. HSE06 calculations also improve the accuracy of the band gap especially for the relatively small-gap materials, such as SrTiO_3 . The HSE06-calculated band gap of SrTiO_3 is 3.28 eV, in good agreement with the experimental value of 3.3 eV.⁴¹ However, the Mn^{4+} emission energies calculated by HSE06 are still significantly lower than the experimental values as shown in Table II. This shows that including nonlocal correlation effect by using hybrid functionals does not solve the intrinsic problem of DFT as a single-particle ground state theory in describing electronic transitions between multi-electron excited states.

IV. Conclusions

DFT-PBE calculations are performed to calculate the Mn^{4+} emission energies for a large number of oxides and fluorides with diverse crystal structures. The calculations focus on materials with octahedral sites for Mn dopants because the octahedral environment is ideal for stabilizing the 4+ oxidation state for Mn. The PBE calculations underestimate the Mn^{4+} emission energy but produce a trend, consistent with the experimental results, in a large number of Mn^{4+} activated phosphors. The results in this

work show that Mn^{4+} activated phosphors with weak Mn-ligand hybridization (between Mn $3d(t_{2g})$ states and ligand p states) tend to exhibit higher emission energies. The weak hybridization can be caused by long Mn-ligand distance and/or distorted bond angles around the Mn octahedral site. Several new oxide host materials (e.g., Y_2O_3 and $\text{La}_2\text{Zr}_2\text{O}_7$) are found for Mn^{4+} . Their emission energies are higher than those currently known for Mn^{4+} doped oxides and should be closer to that of $\text{Y}_2\text{O}_3:\text{Eu}^{3+}$ (commercial red phosphor for fluorescent lighting). The trends of the Mn^{4+} emission energy observed in this study can be used for searching new Mn^{4+} activated red phosphors.

Acknowledgements

The author is grateful for the stimulating discussion with L. A. Boatner, David J. Singh, S. A. Payne, N. J. Cherepy, A. M. Srivastava, and W. W. Beers. This work is supported by the Critical Materials Institute, an Energy Innovation Hub funded by the U.S. Department of Energy, Office of Energy Efficiency and Renewable Energy, Advanced Manufacturing Office.

¹ K. Biswas and M. –H. Du, Phys. Rev. B, **86**, 014102 (2012).

² M. –H. Du and K. Biswas, J. Lumin. **143**, 710 (2013).

³ A. A. Setlur, R. J. Lyons, J. E. Murphy, N. P. Kumar, and M. S. Kishore, ECS J. Solid State Sci. Tech. **2**, R3059 (2013).

⁴ M. D. Birowosuto and P. Dorenbos, Phys. Stat. Sol. A **206**, 9 (2009).

⁵ P. Dorenbos, J. Lumin. **91**, 91 (2000).

-
- ⁶ P. Dorenbos, *J. Lumin.* **104**, 239 (2003).
- ⁷ N. J. Cherepy, S. A. Payne, S. J. Asztalos, G. Hull, J. D. Kuntz, T. Niedermayr, S. Pimputkar, J. J. Roberts, R. D. Sanner, T. M. Tillotson, E. van Loef, C. M. Wilson, K. S. Shah, U. N. Roy, R. Hawrami, A. Burger, L. A. Boatner, W. –S. Choong, and W. W. Moses, *IEEE Trans. Nucl. Sci.* **56**, 873 (2009).
- ⁸ W. W. Moses, *Nucl. Instrum. Met. Phys. Res. A* **487**, 123 (2002).
- ⁹ M. G. Brik, A. M. Srivastava, *J. Lumin.* **133**, 69 (2013).
- ¹⁰ M. G. Brik and A. M. Srivastava, *Opt. Mat.* **35**, 1251 (2013).
- ¹¹ P. W. M. Jacobs, *J. Phys. Chem. Sol.* **52**, 35 (1991).
- ¹² A. Ranfagni, D. Mugnai, M. Bacci, G. Viliani, and M. P. Fontana, *Adv. Phys.* **32**, 823 (1983).
- ¹³ W. Beall Fowler, “Physics of color centers”, edited by W. Beall Fowler, Academic Press Inc., New York (1968).
- ¹⁴ A. M. Srivastava and T. J. Sommerer, *ECS’s INTERFACE* **2**, 28 (1998).
- ¹⁵ A. A. Setlur, E. V. Radkov, C. S. Henderson, J. –H. Her, A. M. Srivastava, N. Karkada, M. S. Kishore, N. P. Kumar, D. Aesram, A. Deshpande, B. Kolodin, L. S. Grigorov, and U. Happek, *Chem. Mater.* **22**, 4076 (2010).
- ¹⁶ G. B. Loutts, M. Warren, L. Taylor, R. R. Rakhimov, H. R. Ries, G. Miller III, M. A. Curley, N. Noginova, N. Kukhtarev, H. J. Caulfield, and P. Venkateswarlu, *Phys. Rev. B* **57**, 3706 (1998).
- ¹⁷ Ya Zhydachevskii, D. Galanciak, S. Kobayakov, M. Berkowski, A. Kamińska, A. Suchocki, Ya Zakharko, and A. Durygin, *J. Phys.: Condens. Matter* **18**, 11385 (2006).

-
- ¹⁸ Ya Zhydachevskii, A. Durygin, A. Suchocki, A. Matkovskii, D. Sugak, P. Bilski, and S. Warchol, *Nucl. Instrum. Methods B* **227**, 545 (2005).
- ¹⁹ Z. Bryknar, V. Trepakov, Z. Potucek, L. Jastrabik, *J. Lumin.* **87**, 605 (2000).
- ²⁰ S. Geschwind, P. Kisliuk, M. P. Klein, J. P. Remeika, D. L. Wood, *Phys. Rev.* **126**, 1684 (1962).
- ²¹ A. Brenier, A. Suchocki, C. Pedrini, G. Boulon, and C. Madej, *Phys. Rev. B* **46**, 3219 (1992).
- ²² M. G. Brik, A. M. Srivastava, *ECS J. Sol. State Sci. Tech.* **2** R148 (2013).
- ²³ K. Dunphy and W. W. Duley, *J. Phys. Chem. Solids* **51**, 1077 (1990).
- ²⁴ T. Takahashi, S. Adachi, *J. Electrochem. Soc.* **155**, E183 (2008).
- ²⁵ T. Arai and S. Adachi, *Jp. J. Appl. Phys.* **50**, 092401 (2011).
- ²⁶ Y. K. Xu, S. Adachi, *J. Appl. Phys.* **105**, 013525 (2009).
- ²⁷ Y. Arai and S. Adachi, *J. Lumin.* **131**, 2652 (2011).
- ²⁸ Y. Tanabe and S. Sugano, *J. Phys. Soc. Jp.* **9**, 766 (1954).
- ²⁹ Y. Tanabe and S. Sugano, *J. Phys. Soc. Jp.* **11**, 864 (1956).
- ³⁰ M. G. Brik, N. M. Avram, and C. N. Avram, in “Optical Properties of 3d-ions in crystals”, ed. N. M. Avram and M. G. Brik, Tsinghua University Press, Beijing and Springer-Verlag Berlin Heidelberg (2013).
- ³¹ W. Kohn and L. J. Sham, *Phys. Rev.* **140**, A1133 (1965).
- ³² J. P. Perdew, K. Burke, and M. Ernzerhof, *Phys. Rev. Lett.* **77**, 3865, (1996).
- ³³ J. Heyd, G. E. Scuseria, and M. Ernzerhof, *J. Chem. Phys.* **118**, 8207 (2003).
- ³⁴ J. Heyd, G. E. Scuseria, and M. Ernzerhof, *J. Chem. Phys.* **125**, 224106 (2006).

-
- ³⁵ G. Kresse and J. Furthmüller, *Phys. Rev. B* **54**, 11169 (1996).
- ³⁶ G. Kresse and D. Joubert, *Phys. Rev. B* **59**, 1758 (1999).
- ³⁷ In Ga_2O_3 , there are two inequivalent Ga sites, one octahedral and one tetrahedral site. The octahedral site is chosen for Mn^{4+} substitution. The energetics of Mn and its possible oxidation state on the tetrahedral site are not studied.
- ³⁸ Y_2O_3 and In_2O_3 have the same bixbyite crystal structure (Ia-3, space group 206) and have two inequivalent cation sites with S_6 and C_2 symmetries; both are six-fold coordinated. In the emission energy calculations, Mn^{4+} is placed on the S_6 site. The S_6 site is energetically more favorable for Mn^{4+} substitution than the C_2 site by 0.42 and 0.29 eV for Y_2O_3 and In_2O_3 , respectively.
- ³⁹ There are two inequivalent sites for Si in Na_2SiF_6 , i.e., 1a and 2d sites. The 2d site is more favorable for Mn substitution than the 1a site by 0.1 eV. Mn^{4+} ions on both 1a and 2d sites have octahedral environments and their calculated emission energies are 1.02 and 1.03 eV, respectively.
- ⁴⁰ D. J. Singh, G. E. Jellison, Jr., and L. A. Boatner, *Phys. Rev. B* **74**, 155126 (2006).
- ⁴¹ J. Robertson, *J. Vac. Sci. Tech. B* **18**, 1785 (2000).
- ⁴² Y. Kitaoka, K. Nakamura, T. Akiyama, T. Ito, M. Weinert, and A. J. Freeman, *Phys. Rev. B* **87**, 205113 (2013).
- ⁴³ T. Archer, C. D. Pemmaraju, S. Sanvito, C. Franchini, J. He, A. Filippetti, P. Delugas, D. Puggioni, V. Fiorentini, R. Tiwari, and P. Majumdar, *Phys. Rev. B* **84**, 115114 (2011).
- ⁴⁴ J. Hong, A. Stroppa, J. Íñiguez, S. Picozzi, and D. Vanderbilt, *Phys. Rev. B* **85**, 054417 (2012).